



基于DIRC方法对于高定时精度的PID探测器设计与BESIII上对于 $\Sigma^0 \to \Lambda e^+ e^-$ 超子辐射衰变的研究

Teng Ma

Supervisor: Haiping Peng

Thesis Proposal Report

October 1, 2025

目录





DIRC-like探测器的研究

- ◆ 选题依据
- ◆ LHCb Upgrade II中TORCH探测器的研究内容与进展
- ◆ STCF桶部BTOF探测器的研究内容与进展



BESIII上超子辐射衰变 $\Sigma^0 \to \Lambda e^+ e^-$ 的研究

- ◆ 选题依据
- ◆ 研究进展



研究计划与安排

研究背景





粒子物理标准模型 — 被实验证实的最成功模型,但仍然存在一些"缺陷"

- > 引力、暗物质和暗能量解释困难
- > 宇宙正反物质不对称现象
- ▶ μ 子反常磁矩疑难
- ▶ 中微子质量问题……

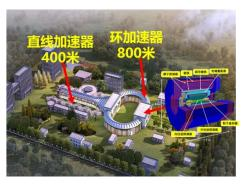
高能量前沿,通过在高能区产生新粒子和新现象 直接发现新物理



大型强子对撞机 (LHC)

- 13 TeV p-p 对撞
- 直接寻找尚未发现的新粒子
- 成果:发现希格斯粒子……

高亮度前沿,通过对重味夸克与轻子和玻色子的 精确测量发现新物理迹象



超级陶粲装置 (STCF)

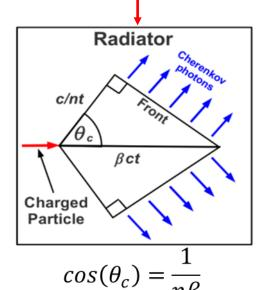
- 峰值亮度 0.5-1×10³⁵ cm⁻²s⁻¹
- 能量区间 Ecm = 2-7 GeV
- 极化束流(Phase II)

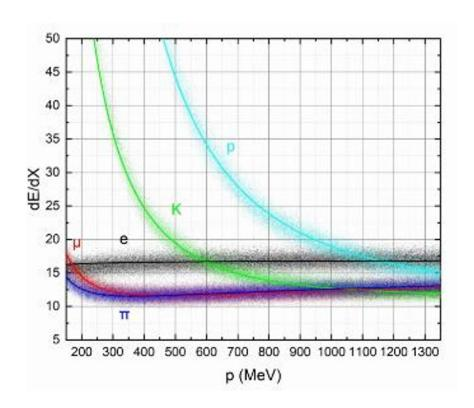
带电粒子鉴别方法



基于质量鉴别粒子

- ➤ 电离能损dE/dx (低动量)
- PID探测器 两个备选 方案
- > 飞行时间TOF
- 切伦科夫辐射和穿越辐射





带电粒子鉴别方法



飞行时间探测器(TOF)

- 相同动量下,使用不同质量粒子在相同距离内的飞行时间差实现粒子鉴别
- ▶ 闪烁体探测器,多气隙阻性板 (MRPC)等
- 本征时间分辨较差,难以压制高亮度下的本底
- 难以鉴别高动量下的粒子

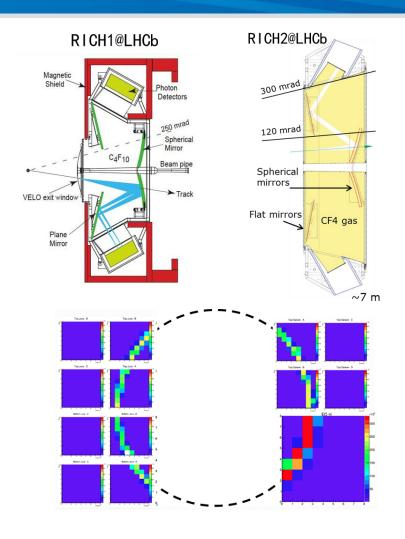
BESIII	Plastic scintillator	~100ps	
	MRPC	~60ps	
BELLE Scintillator		~100ps	

成像型切伦科夫探测器

- > 通过探测高能带电粒子在介质中产生的切伦科夫辐射光子实现粒子鉴别
- 粒子鉴别能力强,动量覆盖范围宽
- ➤ 环形成像切伦科夫探测器(RICH)
- ➤ 内全反射型切伦科夫探测器 (DIRC)

RICH探测器





RICH@LHCb

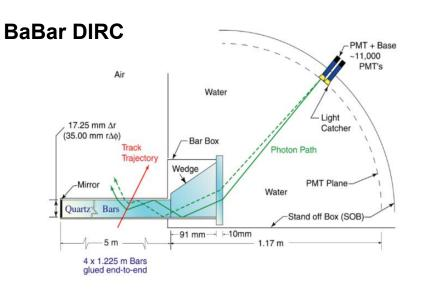
- ➤ 气凝胶辐射体, CF₄ (RICH1) 与 C₄F₁₀ (RICH2)
- 使用球面镜加平面镜聚焦与传递光路
- ▶ 角分辨:
 - √ ~1.66 mrad @ RICH1
 - √ ~0.66 mrad @ RICH2
- ▶ 动量覆盖范围:
 - ✓ 2~60 GeV/c @ RICH1
 - ✓ 15~100 GeV/c @ RICH2
- ✓ 粒子鉴别方法:基于图像识别的极大似然法

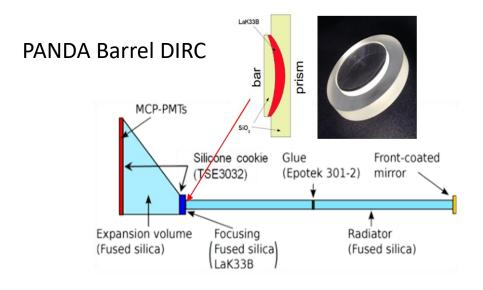
DIRC探测器



DIRC (Detection of Internally Reflected Cherenkov light) 探测器特征

- 内全反射型切伦科夫辐射体,同时作为光导
- 辐射体使用熔融石英板,光子传播角度固定,重建原理简单
- ➤ 表面粗糙度与平整度低 (~1nm), 保证传播方向一致并减少光子损失
- > 基于图像识别的极大似然法鉴别粒子

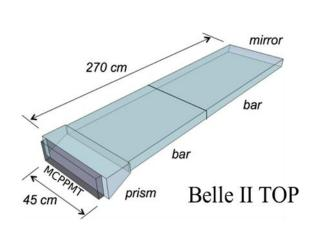


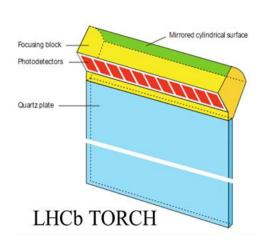


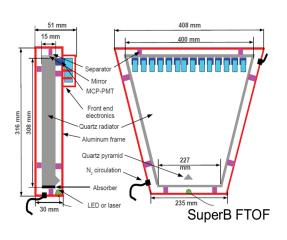
DIRC-like探测器



- 偏重于时间探测,通过时间信息实现鉴别
- ▶ 选用先进光子探测器件MCP-PMT实现超高定时精度







- ▶ Belle II iTOP通过测量光子传输时间,LHCb TORCH与SuperB FTOF通过测量粒子的飞行时间来实现粒子鉴别
- 时间性能优异,结构紧凑,运行维护简单,抗辐照能力强,耐高计数率
- 超高定时精度可有效压低本底带来的影响

目录





DIRC-like探测器的研究

- ◆ 选题依据
- ◆ LHCb Upgrade II中新型TORCH探测器的研究内容与进展
- ◆ STCF桶部BTOF探测器的研究内容与进展



BESIII上超子辐射衰变 $\Sigma^0 \to \Lambda e^+ e^-$ 的研究

- ◆ 选题依据
- ◆ 研究进展



研究计划与安排

LHCb Upgrade II



LHCb Upgrade II是欧洲大型强子对撞机LHC上底夸克探测系统LHCb的基于第一次升级改进后的第二次重大升级项目

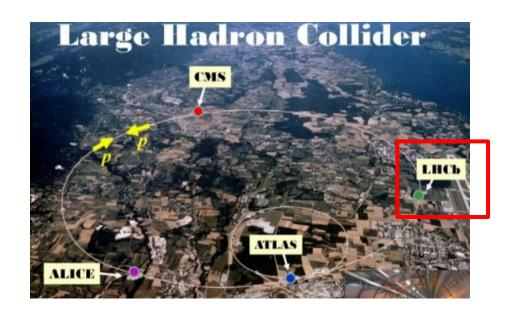
- 具备高瞬时亮度运行能力,快速时间响应能力并采用抗辐照技术,从而获得更强大的数据采集能力
- 是重味物理领域研究的重要平台,还支持味物理领域外的许多研究,如暗物质粒子直接搜寻、强子谱学与重离子碰撞中的QCD研究等

LHCb Upgrade I

- □ 瞬时亮度 2×10³³ cm⁻²s⁻¹
- 目标数据 50fb⁻¹

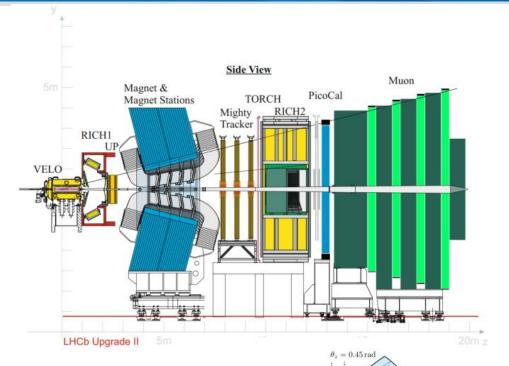
LHCb Upgrade II

- □ 瞬时亮度 ~10³⁴ cm⁻²s⁻¹
- 目标数据 300fb⁻¹
- □ 快速时间响应能力与抗辐照技术

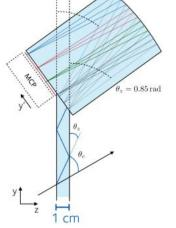


整体布局



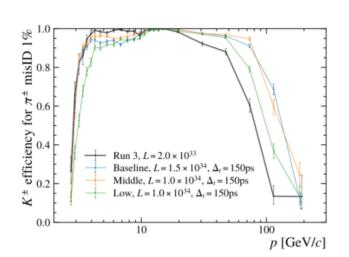


TORCH示意图:



LHCb Upgrade II 粒子鉴别系统

- Arr 在大范围动量内实现 $\pi/K/p$ 的精确鉴别 (3 σ)
- ➤ 由RICH1, RICH2以及新型的DIRC-like切伦科夫探测器TORCH组成
- ➢ RICH无法提供<10GeV/c的K/p</p>
 鉴别能力,需要TORCH弥补
- ▶ 要求具备高精度定时能力以抑制本底



TORCH时间分辨



TORCH要求快速时间响应,预期单光子本征时间分辨~70ps,光子数~25

$$\sigma_{SPE}^2 \sim \left(\frac{\sigma_{elec}}{\sqrt{N_{p.e.}}}\right)^2 + \left(\frac{\sigma_{TTS}}{\sqrt{N_{p.e.}}}\right)^2 + \left(\frac{\sigma_{prop} \cdot t_{prop}}{\sqrt{N_{p.e.}}}\right)^2$$

- $ightharpoonup \sigma_{elec}$ 电子学定时精度
- ho σ_{TTS} 光电器件渡越时间涨落
- ho $\sigma_{prop} \cdot t_{prop}$ 表征色散效应随光子传播时间增大的贡献

当前TORCH所面临的挑战:

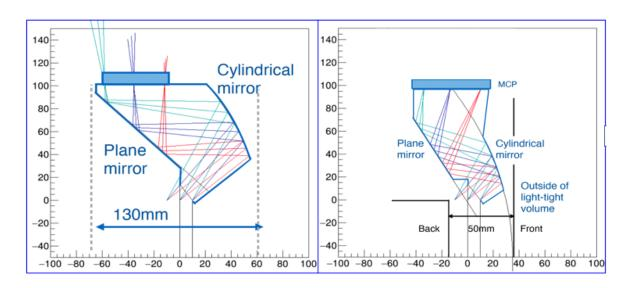
- > 光子数目难以达标
- ▶ 与TORCH预留空间不适配

新型TORCH探测器

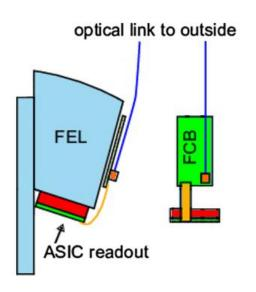


基于PANDA端盖DIRC探测器的技术对于TORCH的几何改进

- ➤ 解决原有TORCH方案的几何难以与预留的尺寸与机械结构适配的问题
- 避免光子数因二次镜面反射导致的额外损失
- 采用电介质材料键合来连接聚焦体与石英板以减少光子数损失
- 需要配套的独立Geant4模拟与重建算法
- 需要进行样机关键技术的验证与实验测试

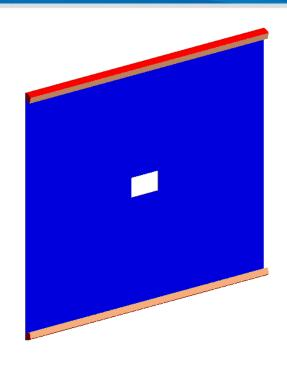


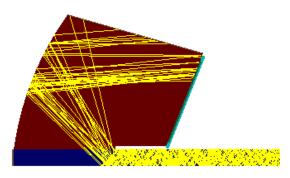
TORCH-PANDADIRC



Geant4模拟



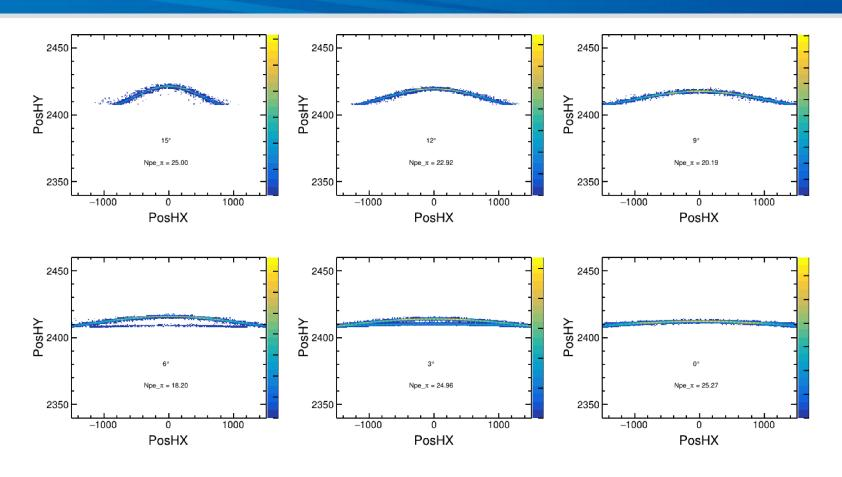




- ▶ 基于实际全尺寸的建模
- ▶ 尚未考虑前端探测器的影响
- ▶ 单块石英板尺寸2500mm * 660mm * 10mm
- > 未引入滤波系统以增加光子数
- 在石英板与聚焦模块间添加一狭窄空隙以增加 大角度光子击中

模拟结果与光子数



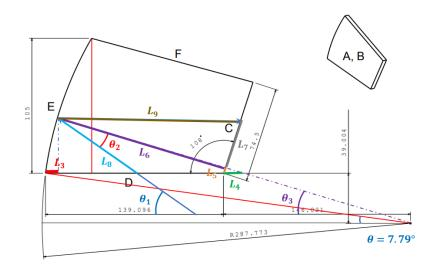


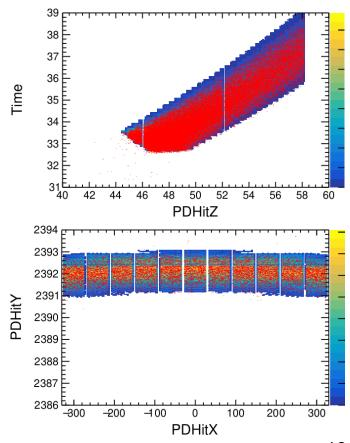
▶ 需要进一步调整几何以减少打到吸收层的大角度光子

新型TORCH重建算法



- ▶ 计算单径迹理论PDF去计算似然值
- ➤ 当前正方向传播光子的重建pattern与模拟结果吻合
- 关键参数接口化设计,方便更改
- 未来将考虑反方向传播的切伦科夫光重建



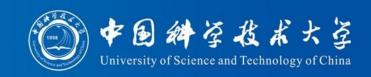


样机技术论证



- ▶ 石英板@北玻所
 - 加工粗糙度要求<1nm, 平整度要求<3μm
 - 2500*660*10mm熔融石英板,加工粗糙度最佳可达0.5nm, 平整度~1μm
 - 需要考虑粗糙度与平整度测量 (STCF BTOF样机已有测量经验)
- ➤ MCP-PMT@Photek
 - 预期寿命>5C/cm² (已满足)
 - 可实现单光子PMT30ps的时间分辨与<0.1mm的空间分辨能力
 - 串扰现象有待测量
- ➤ 电子学系统@NINO板+HPTDC芯片组合
 - 预期设计要求定时精度<50ps (已实现)
 - 需要进行宇宙线测试
- 石英板与聚焦体键合技术@北玻所
 - 熔融石英材料表面间通过分子力键合
 - 目前北玻所键合材料尺寸<150mm(直径)
 - 需要提升工艺+材料分割键合(如果分割材料,需要设计调整和G4模拟)

目录





DIRC-like探测器的研究

- ◆ 选题依据
- ◆ LHCb Upgrade II中新型TORCH探测器的研究内容与进展
- ◆ STCF桶部BTOF探测器的研究内容与进展



BESIII上超子辐射衰变 $\Sigma^0 \to \Lambda e^+ e^-$ 的研究

- ◆ 选题依据
- ◆ 研究进展



研究计划与安排

超级陶築装置 (STCF) (Diversity of Science and Technology of China

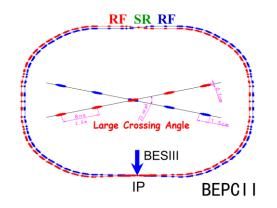


超级陶粲装置是中国未来的高亮度正负电子对撞机项目

- ▶ 更高的亮度与更广泛的能量区间
- ➤ 是研究陶-粲物理、QCD、新型强子以及寻找新物理的重要平台

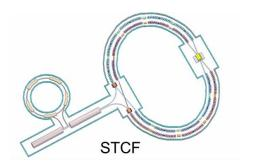
北京正负电子对撞机(BEPCII)

- 峰值亮度 1×10³³ cm⁻²s⁻¹
- 能量区间 E_{cm} = 2-4.6 GeV
- 无极化



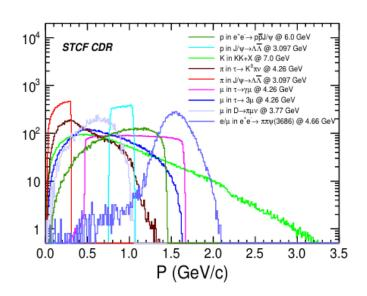
超级陶粲装置(STCF)

- 峰值亮度 0.5-1×10³⁵ cm⁻²s⁻¹
- 能量区间 E_{cm} = 2-7 GeV
- 极化束流(Phase II)



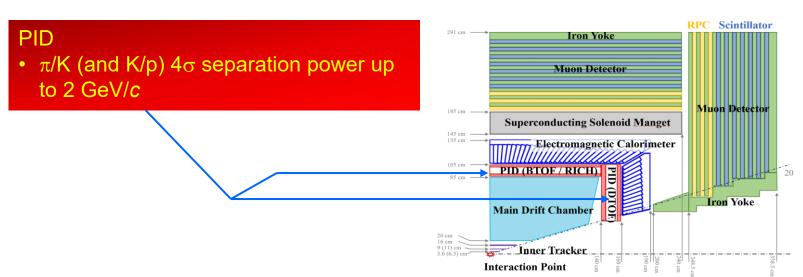
探测器布局





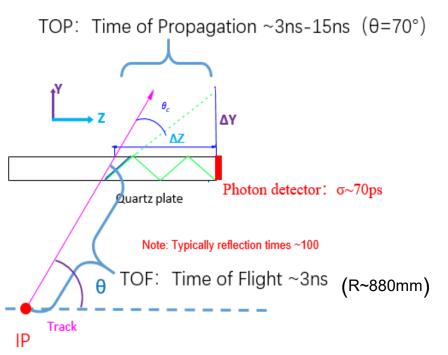
超级陶粲对粒子鉴别探测器需求

- 2GeV/c π/K/p ~4σ (即2%误鉴别率下, 97%鉴别 效率)
- ▶ 结构紧密: <20cm (为量能器预留空间)
- ▶ 物质量: < 0.3X₀ (减少能量畸变)
- ▶ 本底计数率: ~13 kHz/通道 (1倍本底)
- 桶部当前默认方案为BTOF方案,通过DIRC技术实现 4σ粒子鉴别



BTOF方案简介





- ▶ 与IP点距离约为880mm, TOF与TOP呈互补关系 (需进行模拟研究分析)
- ▶ 使用新型MCP-PMT实现高定时精度(70ps)
- 色散效应明显,在TOP较大时不可忽略,可通过 滤波实现较好的单光子时间分辨,但同时会减 少光子数(当前采用400nm滤波)
- 不需要聚焦系统,探测器结构更为紧凑
- STCF端盖的DTOF探测器也采用成熟的DIRC技术, 且两者电子读出系统高度相似,维护也较为方 便
 21

BTOF时间分辨



$$\sigma_{tot}^2 \sim \sigma_{trk}^2 + \sigma_{T_0}^2 + \left(\frac{\sigma_{elec}}{\sqrt{N_{p.e.}}}\right)^2 + \left(\frac{\sigma_{TTS}}{\sqrt{N_{p.e.}}}\right)^2 + \left(\frac{\sigma_{det}}{\sqrt{N_{p.e.}}}\right)^2$$

- *N_{p.e.}*光电子数目
- σ_{trk} 径迹重建误差(~10ps)
- σ_{T_0} 参考时间误差(~40ps)
 - 即東团对撞时间

若采用传统TOF方法进行粒子鉴别,若取L=1.1m,2GeV/c下,实现 4σ π/K 区分度的时间分辨需 $\sigma\sim26ps<\sigma_{T_0}$

- BTOF本征时间分辨
 - $ightharpoonup \sigma_{elec}$ 电子学定时精度(~10ps)
 - $ightharpoonup \sigma_{TTS}$ 光电器件渡越时间涨落(~70ps)
 - $ightharpoonup \sigma_{det}$ BTOF重建误差

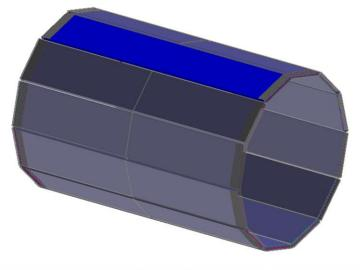
提升时间分辨途径

- > 对单光子精确重建
- ▶ 提高单光子本征时间分辨
- ▶ 提高光电子数目

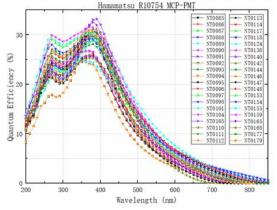
BTOF模拟

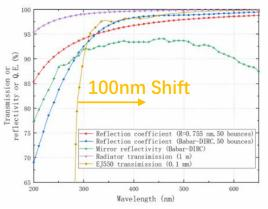


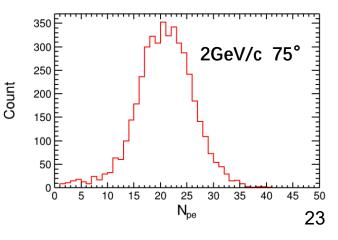
基于高性能离线软件系统OSCAR下的BTOF模拟程序来研究验证其预期性能



- ➤ 石英板尺寸1350mm * 450mm * 20mm
- ➤ 铝蜂窝板光学屏蔽盒~5mm
- ▶ 光电器件4*4,像素尺寸4.8mm * 4.8mm
- 径迹使用外推算法考虑前端探测器与外壳的物质量影响
- > 两块石英板相互拼接以提高大角度径迹的光电子数



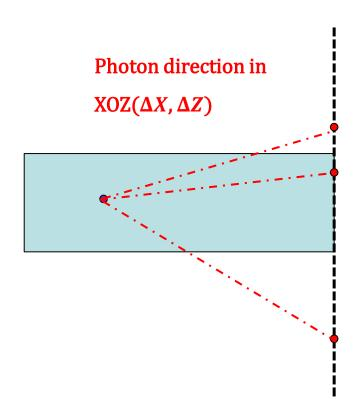




BTOF重建(一维算法) (如今日科学技术大学 University of Science and Technology of China



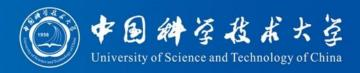
Timing Method



$$TOF = T - TOP - T_0 = T - \frac{L\overline{n_g}}{c} - T_0$$

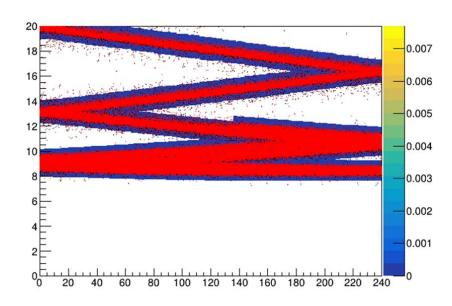
- \rightarrow 加入数字化 $(\sigma_{T_0}, \sigma_{TTS}$ 等) 的影响
- 存在多种可能路径
- ▶ 对于每种可能路径计算其TOP,从而重建 出TOF
- 挑选与预期假设(通过外推径迹得到)最接近 的可能作为重建路径
- ▶ 加入全反射判选条件

BTOF重建(二维算法)



Imaging Method

- ightharpoonup 加入数字化 $(\sigma_{T_0}, \sigma_{TTS}$ 等) 的影响
- ▶ 对于每个事例根据径迹方向与切伦科夫角计算出切伦科夫光的T-Ch二维分布概率 图(T=TOF+TOP)
- ▶ 相比于一维算法引入空间坐标维度
- 加入通道死时间修正

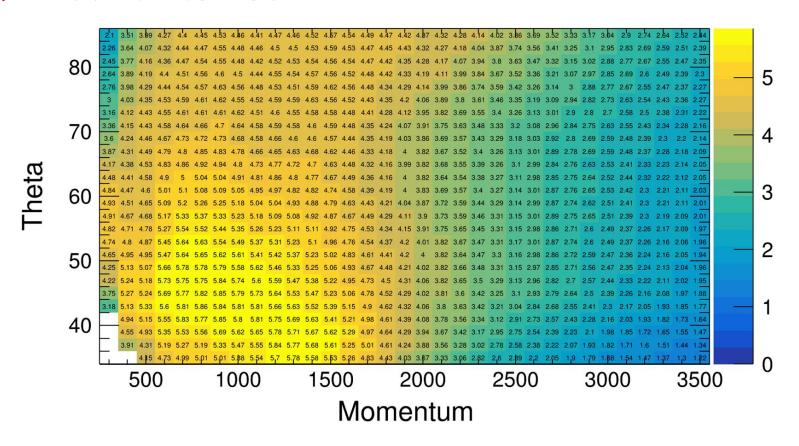


Comparison of calculated PDF and simulation

BTOF重建性能



π/K 二维算法鉴别性能图

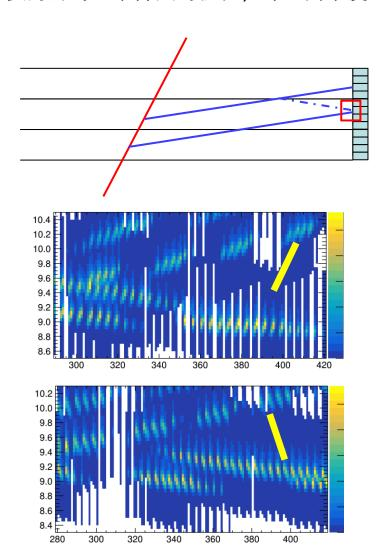


- ightharpoonup 在2GeV以下可以满足STCF对于PID性能要求($\varphi \sim (0, 2\pi)$)
- ▶ 在2GeV某些点略有差距,且与一维时间算法难以拉开性能差距,期待后续优化

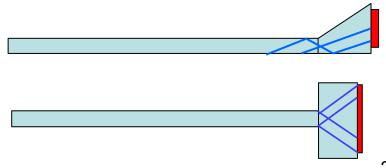
BTOF后续优化路线



主要为针对二维算法的优化,即空间维度上的优化



- ➢ 光子在Y方向根据反射次数的奇偶性有两组 pad分布,在PDF上的堆叠会降低在空间坐标 中的区分能力
- ▶ 计划方案为在原石英板与PMT之间加装一个 大尺寸光导,用以统一最终切伦科夫光的传 播方向



BTOF后续优化路线

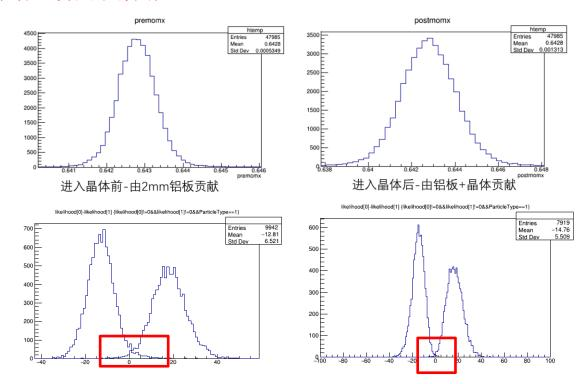


对于多次散射的优化

多次散射对于击中位置的影响显著大于预期

Standa I one模拟下进入 晶体前后径迹x方向的 分布

在初步将前后的动量方 向范围限制在±0.3可以 获得更好的重建效果



由于BTOF光子传播路程极长,取保守估计TOP=1.5m,则3mrad的散射角度偏差会导致PMT阵列平面上偏差距离达到约5mm,几乎相当于一个像素尺寸的距离

目录





DIRC-like探测器的研究

- ◆ 选题依据
- ◆ LHCb Upgrade II中新型TORCH探测器的研究内容与进展
- ◆ STCF桶部BTOF探测器的研究内容与进展



BESIII上超子辐射衰变 $\Sigma^0 \to \Lambda e^+ e^-$ 的研究

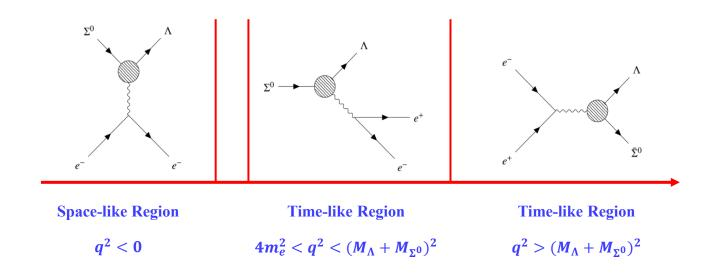
- ◆ 选题依据
- ◆ 研究进展



研究计划与安排

选题依据





形状因子

- 探究强子内部结构的重要物理量
- 揭示强子内部电荷与磁矩分布
- 描述相互作用随能量尺度(动量转移)的变化

研究意义

- 该过程分支比仅有理论计算,缺少实验测量结果
- ho 低动量转移区间的hoΛ类时形状 因子尚无测量结果
- BESIII拥有最大的具备高重子对 分支比的 J/ψ 数据集

预期目标

- $Σ^0 → Λe^+e^-$ 过程分支比
- Σ⁰Λ低动量转移区间类时形状因子
- $\Sigma^0\Lambda$ 跃迁磁矩

目录





DIRC-like探测器的研究

- ◆ 选题依据
- ◆ LHCb Upgrade II中新型TORCH探测器的研究内容与进展
- ◆ STCF桶部BTOF探测器的研究内容与进展



BESIII上超子辐射衰变 $\Sigma^0 \to \Lambda e^+ e^-$ 的研究

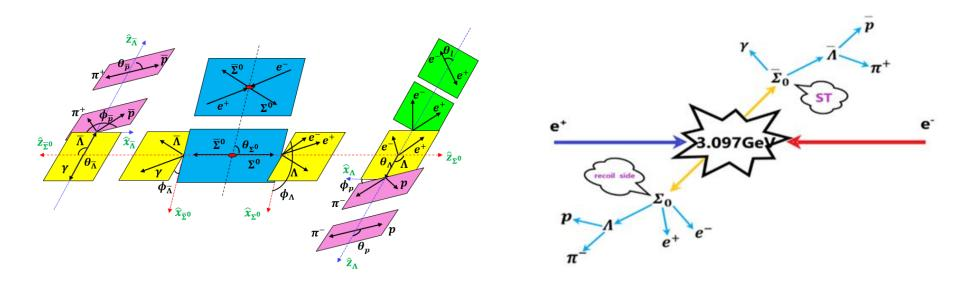
- ◆ 选题依据
- ◆ 研究进展



研究计划与安排

分析策略



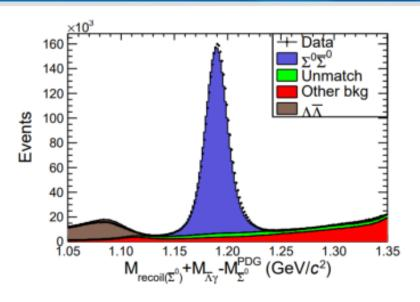


单双标分析策略

- ▶ 衰变链 $J/\psi \to \Sigma^0 \bar{\Sigma}^0 \to \Lambda \bar{\Lambda} \gamma e^+ e^- \to p \bar{p} \pi^+ \pi^- \gamma e^+ e^-$,包含电荷共轭道
- ightharpoonup 单标端(ST), $\bar{\Sigma}^0 \to \bar{p}\pi^+\gamma$, $\Sigma^0 \to anything$
- ightharpoonup 双标端(DT),ightharpoonup0 ightharpoonup7 ightharpoonup7 ightharpoonup7 ightharpoonup7 ightharpoonup7 ightharpoonup7 ightharpoonup7 ightharpoonup7 ightharpoonup7 ightharpoonup8 ightharpoonup7 ightharpoonup8 ightharpoonup9 ightharpoonup9
- Arr N_{ST} 与 N_{DT} 为单双标信号事例数, ε_{ST} 和 ε_{DT} 为单双标信号效率.

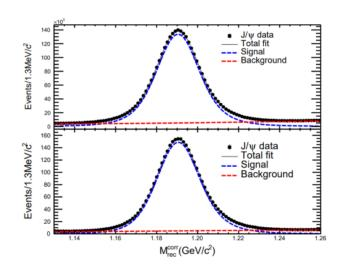
单标结果







- ▶ 信号区间内没有峰本底分布
- ▶ 本底包含非信号过程与光子truth信息不匹配的信号过程



▶ 利用单标端∑⁰反冲质量谱提取信号

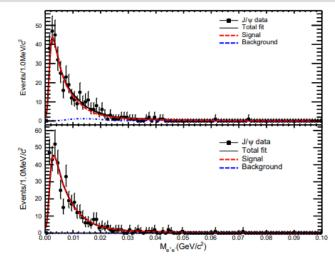
▶ 信号PDF:信号蒙卡形状卷积高斯函数

➤ 本底PDF: 二阶切比雪夫多项式

Modes	$J/\psi \to \Sigma^0 \bar{\Sigma}^0, \bar{\Sigma}^0 \to \bar{\Lambda}\gamma, \Sigma^0 \to anything$	$J/\psi \to \Sigma^0 \bar{\Sigma}^0, \Sigma^0 \to \Lambda \gamma, \bar{\Sigma}^0 \to anything$
ST Yields	2916940 ± 2655	3225220 ± 2645
ST efficiency (%)	36.46	38.13
$\mathcal{B}_{J/\psi\to\Sigma^0\bar{\Sigma}^0}(\times 10^{-3})$	1.242 ± 0.001	1.311 ± 0.001

双标结果





$$\begin{split} \Gamma_{\Sigma^0 \to \Lambda e^+ e^-} &= \int d\Gamma_{\Sigma^0 \to \Lambda e^+ e^-} / dq^2 dq^2 = \int |G_M(0)|^2 W(q^2) dq^2 \\ &= \Gamma_{total} \mathcal{B}_{\Sigma^0 \to \Lambda e^+ e^-}, \end{split}$$

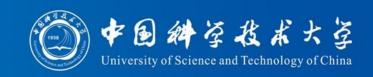
$$\mathscr{B}_{\Sigma^0 \to \Lambda e^+ e^-} = \frac{N_{DT}}{N_{ST}} \times \frac{\varepsilon_{ST}}{\varepsilon_{DT}} \times \frac{1}{\mathscr{B}_{\Lambda \to p\pi^-}}$$

- ▶ 利用e⁺e⁻不变质量谱提取信号
- ightharpoonup 本底过程来源于ightharpoonup0 ightharpoonupΛγ过程
- 信号与本底过程均使用蒙卡形状描述

Modes	$\Sigma^0 \to \Lambda e^+ e^-$	$\bar{\Sigma}^0 \to \bar{\Lambda} e^+ e^-$
ST Yields	2916940 ± 2655	3225220 ± 2645
ST efficiency(%)	36.46	38.13
DT Yields	347.93 ± 23.19	405.05 ± 20.11
DT efficiency(%)	1.04	1.12
Individual $\mathcal{B}_{\Sigma^0 \to \Lambda e^+ e^-}(\times 10^{-3})$	$6.34 \pm 0.44_{\rm stat.} \pm 0.21_{\rm sys.}$	$6.29 \pm 0.33_{\rm stat.} \pm 0.14_{\rm sys.}$
Simultaneous $\mathcal{B}_{\Sigma^0 \to \Lambda e^+ e^-}(\times 10^{-3})$	$6.32\pm0.25_{\rm s}$	$_{ m tat.} \pm 0.18_{ m sys.}$
Individual $G_{\rm M}(0)$	$2.13 \pm 0.09_{\rm stat.} \pm 0.05_{\rm sys.}$	$2.12 \pm 0.06_{\rm stat.} \pm 0.04_{\rm sys.}$
Simultaneous $G_{\rm M}(0)$)	$2.13\pm0.04_{\rm s}$	$_{ m tat.} \pm 0.05_{ m sys.}$
Individual $\mu/(\frac{e}{2m_p})$	$1.74 \pm 0.07_{\rm stat.} \pm 0.03_{\rm sys.}$	$1.73 \pm 0.05_{\rm stat.} \pm 0.02_{\rm sys.}$
Simultaneous $\mu/(\frac{e}{2m_{\rm p}})$	$1.74\pm0.03_{\rm s}$	$_{ m tat.} \pm 0.03_{ m sys.}$
$\Gamma_1 = \Lambda \gamma$	100 %	
$\Gamma_2 = \Lambda \gamma \gamma$	< 3 %	90%

 5×10^{-3}

目录





DIRC-like探测器的研究

- ◆ 选题依据
- ◆ LHCb Upgrade II中TORCH探测器的研究内容与进展
- ◆ STCF桶部BTOF探测器的研究内容与进展



BESIII上超子辐射衰变 $\Sigma^0 \to \Lambda e^+ e^-$ 的研究

- ◆ 选题依据
- ◆ 研究进展



研究计划与安排

研究计划与安排



● 目前已经完成

- TORCH新方案初步几何建模与模拟
- BTOF设计及初步模拟
- BTOF重建算法、粒子鉴别算法开发与性能分析
- BESIII物理分析draft已完成并且即将进入CWR
- 2026~2027年完成
 - TORCH新方案全部重建算法与性能分析
 - TORCH新方案样机关键技术实验与测试
 - BTOF重建算法优化
 - BESIII物理分析文章投稿
- 2027年完成
 - 撰写毕业论文,准备毕业答辩





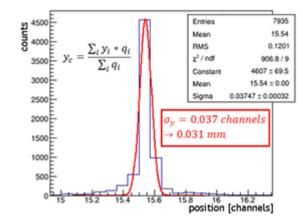
Back UP

TORCH PMT空间分辨 (Diversity of Science and Technology of China

For TORCH, the proposed solution is to use a structured multi-layer ceramic readout anode, which is a hybrid between a multi-anode detector with direct DC connection from the vacuum envelope to outside of the detector and a charge sharing imaging MCP device. This hybrid anode design capacitively couples the signal from the MCP electron avalanche, collected on a resistive layer inside the vacuum, to anode pads embedded in the ceramic structure. The structure of the hybrid anode is designed to allow for charge sharing between anode pads, allowing the use of charge sharing techniques to increase the detector's spatial resolution beyond the pitch of the anode pads. To perform the charge sharing calculation, a charge measurement at each of the anode's readout pad is needed. The photon's position X_{γ} in one dimension can then be naively calculated from

$$X_{\gamma} = \sum_{i=0}^{n} x_i \frac{q_i}{Q} \tag{3.1}$$

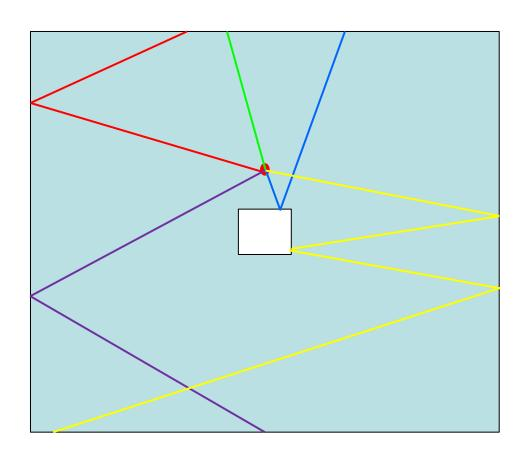
where x_i is the spatial coordinate of a readout pad in one dimension, q_i is the charge collected by that pad and Q is the total charge collected by all readout pads. An ideal algorithm could use weighting of the charge collection efficiency to further improve imaging resolution.



TORCH重建

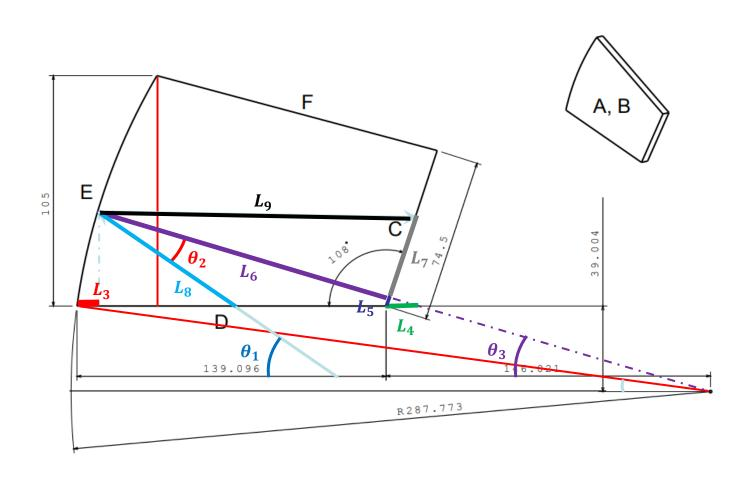


全模型下重建光路较为复杂,需要分别考虑重建算法:



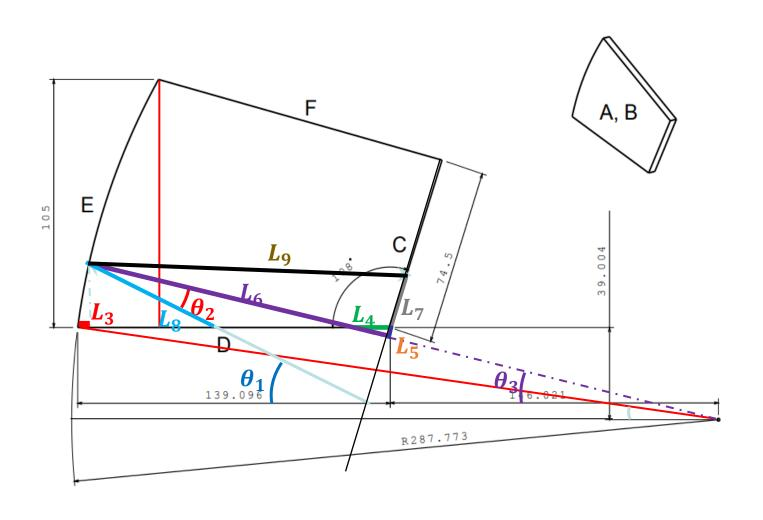
TORCH重建





TORCH重建

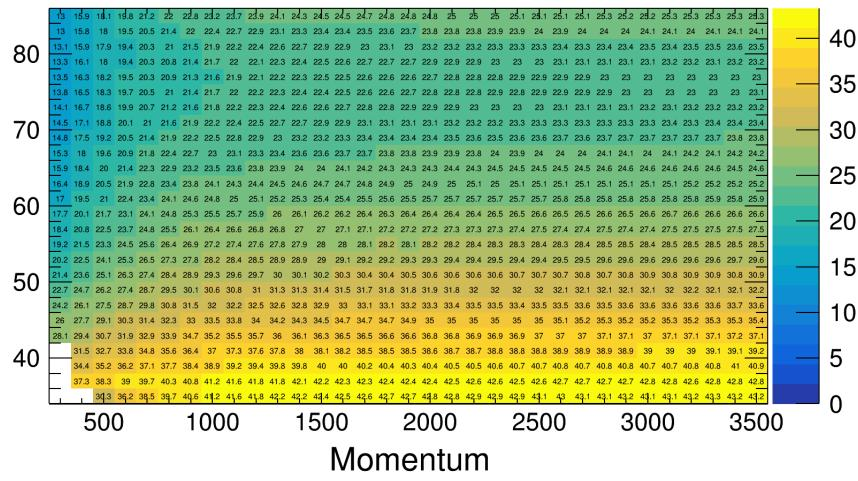




BTOF光子数分布



π 样本



BTOF重建(一维算法)

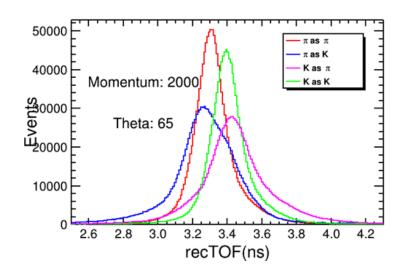


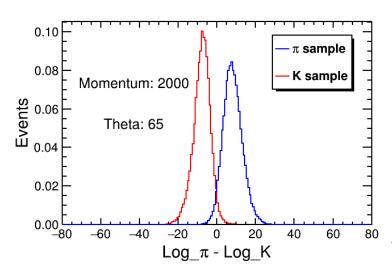
 Δ recTOF (TOF_{rec} – TOF_{hypo}) 的分布使用三高斯模型描述:

ArecTOF

=
$$ratio1 * Gaus1(0, resTOF) + \frac{ratio1}{2} * Gaus2(0.135, sigma1) + (1 - 1.5 * ratio1) * Gaus3(0.05, sigma2)$$

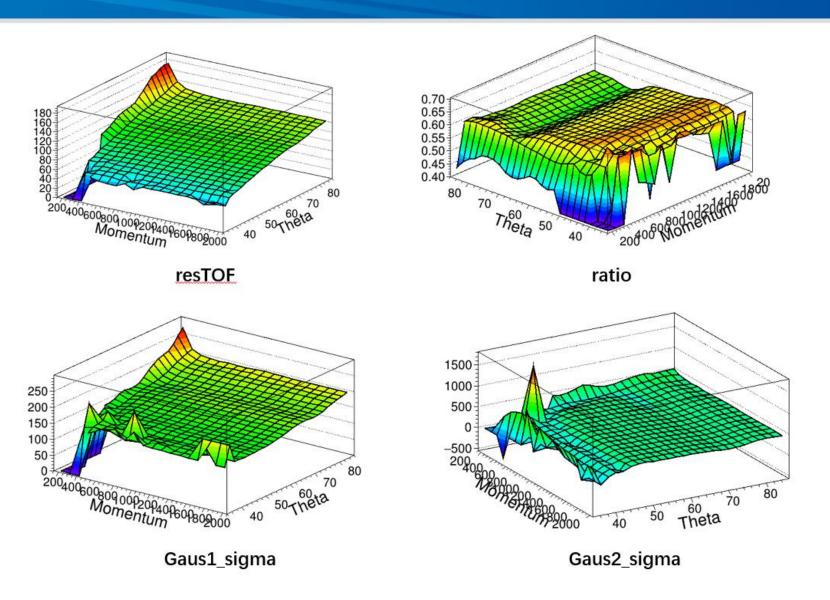
- Gaus1是主峰, Gaus2用来描述渡越时间涨落(TTS)的影响, Gaus3用于描述多次散射效应
- ▶ 以上参数通过拟合不同动量角度下的∆recTOF分布得到,再通过一个关于动量和角度的函数统一描述





ΔrecTOF参数分布

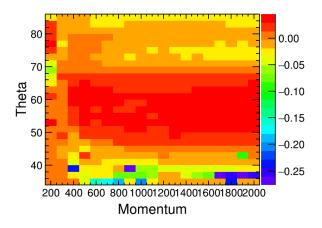




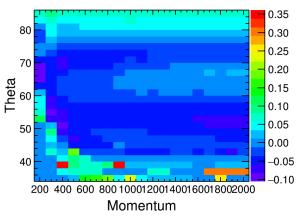
ΔrecTOF参数拟合结果



相对差别

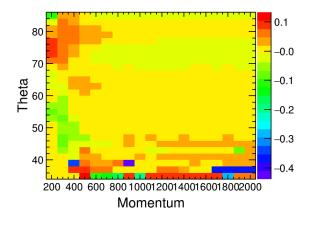


resT0F

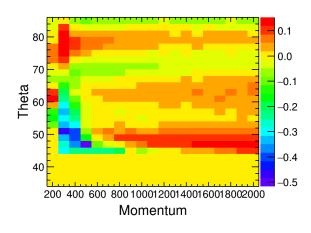


sigma1

sigma2

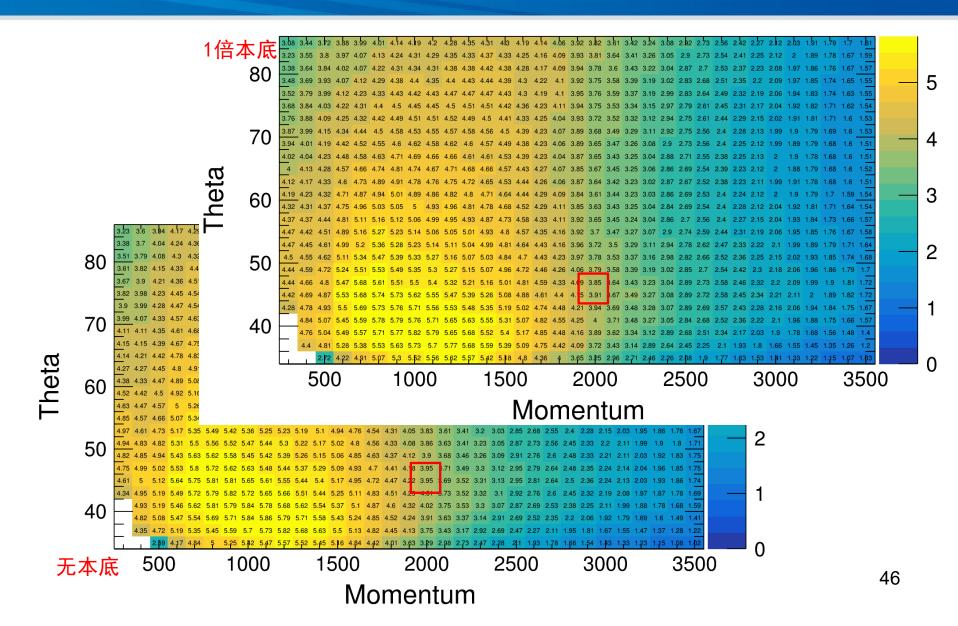


ratio



BTOF本底水平





ST Generator



■ We integrated the $p(\bar{p})$ and $\Lambda(\bar{\Lambda})$ if we tag $\bar{\Sigma}^0(\Sigma^0)$. Then the amplitude for $J/\psi \to \Sigma^0\bar{\Sigma}^0$, $\bar{\Sigma}^0 \to \bar{\Lambda}\gamma$, $\bar{\Lambda} \to \bar{p}\pi^+$, $\Sigma^0 \to anything$ and its conjugate channel is written as:

$$\mathcal{W}_{\Sigma^0} = 2\left(\alpha_-\sqrt{1-\alpha_{\Sigma^0}^2}\sin\Delta\Phi_{\Sigma^0}\sin\theta_{\Sigma^0}\cos\theta_{\Sigma^0}\sin\theta_{\Lambda}\cos\theta_p\sin\phi_{\Lambda} + \alpha_{\Sigma^0}\cos^2\theta_{\Sigma^0} + 1\right)$$

$$\mathcal{W}_{\bar{\Sigma}^0} = 2\left(\alpha_+ \sqrt{1 - \alpha_{\Sigma^0}^2} \sin \Delta \Phi_{\Sigma^0} \sin \theta_{\Sigma^0} \cos \theta_{\Sigma^0} \sin \theta_{\bar{\Lambda}} \cos \theta_p \sin \phi_{\bar{\Lambda}} + \alpha_{\Sigma^0} \cos^2 \theta_{\Sigma^0} + 1\right)$$

- \blacksquare α_{Σ^0} and $\Delta\Phi_{\Sigma^0}$ are the decay parameters to describe $J/\psi \to \Sigma^0 \bar{\Sigma}^0$
- α_- and α_+ are the decay parameters for $\Lambda(\overline{\Lambda}) \to p\pi^-(\overline{p}\pi^+)$
- lacksquare $heta_{\Sigma^0/\overline{\Sigma}^0}$, $heta_{\Lambda/\overline{\Lambda}}$, $heta_{p/\overline{p}}$ are the helicity angles defined in the rest frame of their mother particles.

47

DT Generator



The decay width can be computed as:

$$d\Gamma = \frac{1}{(2\pi)^5} \frac{1}{16M_{\Sigma^0}^2} \mathcal{W}|\vec{p}_l||\vec{p}_{\Lambda}|dqd\Omega_l d\Omega_{\Lambda}$$

■ The complete amplitude is written as [3]:

$$W = \frac{\alpha_{em}^2}{q^4} (q^2 - 4m_l^2) \sum_{\mu,\bar{\nu}=0}^3 \sum_{\mu'=0}^3 \sum_{\bar{\nu}'=0}^3 C_{\mu\bar{\nu}} a_{\mu\mu'}^{\Sigma^0} a_{\bar{\nu}'0}^{\bar{\Lambda}} a_{\bar{\nu},0}^{\bar{\Sigma}^0} a_{\bar{\nu},0}^{\bar{\Lambda}}$$

lacksquare $= 4\pi/137$, q is the four-momentum transfer and m_l is the invariant mass of electron. $C_{\mu\overline{\nu}}$ represents for the polarization and spin correlation of $\Sigma^0\overline{\Sigma}^0$. $a_{\mu\mu'}$ is the decay matrix of hyperons depending on the decay products, which is shown on backup.

[3]: Phys. Rev. D108:016011, 2023.

$C_{\mu\nu}$ matrix



$$C_{\mu\bar{\nu}} \propto \begin{pmatrix} 1 + \alpha_{\psi}\cos^{2}\theta_{1} & 0 & \beta_{\psi}\sin\theta_{1}\cos\theta_{1} & 0\\ 0 & \sin^{2}\theta_{1} & 0 & \gamma_{\psi}\sin\theta_{1}\cos\theta_{1}\\ -\beta_{\psi}^{2}\sin\theta_{1}\cos\theta_{1} & 0 & \alpha_{\psi}\sin^{2}\theta_{1} & 0\\ 0 & -\gamma_{\psi}\sin\theta_{1}\cos\theta_{1} & 0 & -\alpha_{\psi}-\cos^{2}\theta_{1} \end{pmatrix}$$

- \blacksquare $C_{\mu\overline{\nu}}$ is a 4×4 real matrix representing polarizations and spin correlations of the baryons.
- Where the parameters β_{ψ} and α_{ψ} are expressed via α_{ψ} and $\Delta\Phi$ as β_{ψ} =

$$\sqrt{1-\alpha_{\psi}^2}\sin(\Delta\Phi)$$
 and $\gamma_{\psi} = \sqrt{1-\alpha_{\psi}^2}\cos(\Delta\Phi)$

- $\blacksquare \ \alpha_{\psi} = \alpha_{\Sigma^0} = -0.449 \, [5] \quad \Delta \Phi = -0.08 \, [6]$
- lacksquare θ_1 in the electron–positron center-of-momentum (cm) system.

[5]: Phys. Rev. D95, 052003, 2017

[6]: Phys. Rev. Lett. 133, 101902, 2024

Decay matrix



$$A_{\mu\nu}^{\overline{\Sigma}^{0}} = \begin{pmatrix} 1 & 0 & 0 & 0 \\ 0 & 0 & 0 & -sin\theta_{\overline{\Lambda}}cos\phi_{\overline{\Lambda}} \\ 0 & 0 & 0 & -sin\theta_{\overline{\Lambda}}sin\phi_{\overline{\Lambda}} \\ 0 & 0 & 0 & -cos\theta_{\overline{\Lambda}} \end{pmatrix} \qquad B_{\mu\nu}^{\Sigma^{0}} = \sum_{\kappa=0}^{3} R_{\mu\kappa}^{(4)}(\Omega_{l})b_{\kappa\nu}^{em}$$

$$a^{\Lambda}_{\mu\nu} = \begin{pmatrix} 1 & 0 & 0 & \alpha_{\Lambda} \\ \alpha_{\Lambda}sin\theta_{p}cos\phi_{p} & \gamma_{\Lambda}cos\theta_{p}cos\phi_{p} - \beta_{\Lambda}sin\phi_{p} & -\beta_{\Lambda}cos\theta_{p}cos\phi_{p} - \gamma_{\Lambda}sin\phi_{p} & sin\theta_{p}cos\phi_{p} \\ \alpha_{\Lambda}sin\theta_{p}sin\phi_{p} & \gamma_{\Lambda}cos\theta_{p}sin\phi_{p} + \beta_{\Lambda}cos\phi_{p} & -\beta_{\Lambda}cos\theta_{p}sin\phi_{p} + \gamma_{\Lambda}cos\phi_{p} & sin\theta_{p}sin\phi_{p} \\ \alpha_{\Lambda}cos\theta_{p} & -\gamma_{\Lambda}sin\theta_{p} & \beta_{\Lambda}sin\theta_{p} & cos\theta_{p} \end{pmatrix}$$

$$a_{\mu\nu}^{\bar{\Lambda}} = \begin{pmatrix} 1 & 0 & 0 & \alpha_{\bar{\Lambda}} \\ \alpha_{\bar{\Lambda}} sin\theta_{\bar{p}} cos\phi_{\bar{p}} & \gamma_{\bar{\Lambda}} cos\theta_{\bar{p}} cos\phi_{\bar{p}} - \beta_{\bar{\Lambda}} sin\phi_{\bar{p}} & -\beta_{\bar{\Lambda}} cos\theta_{\bar{p}} cos\phi_{\bar{p}} - \gamma_{\bar{\Lambda}} sin\phi_{\bar{p}} & sin\theta_{\bar{p}} cos\phi_{\bar{p}} \\ \alpha_{\bar{\Lambda}} sin\theta_{\bar{p}} sin\phi_{\bar{p}} & \gamma_{\bar{\Lambda}} cos\theta_{\bar{p}} sin\phi_{\bar{p}} + \beta_{\bar{\Lambda}} cos\phi_{\bar{p}} & -\beta_{\bar{\Lambda}} cos\theta_{\bar{p}} sin\phi_{\bar{p}} + \gamma_{\bar{\Lambda}} cos\phi_{\bar{p}} & sin\theta_{\bar{p}} sin\phi_{\bar{p}} \\ \alpha_{\bar{\Lambda}} cos\theta_{\bar{p}} & -\gamma_{\bar{\Lambda}} sin\theta_{\bar{p}} & \beta_{\bar{\Lambda}} sin\theta_{\bar{p}} & cos\theta_{\bar{p}} \end{pmatrix}$$

DT Generator



■ The form factors are included in the decay matrix of $\Sigma^0 \to \Lambda e^+ e^-$, which is described with helicity amplitudes:

$$H_{\frac{1}{2}1}^{V} = \sqrt{2Q_{-}} \left[-F_{1}^{V} + \frac{M_{\Sigma^{0}} + M_{\Lambda}}{M_{1}} F_{2}^{V} \right] = -\sqrt{2Q_{-}} G_{M}$$

$$H_{\frac{1}{2}0}^{V} = \frac{\sqrt{Q_{-}}}{\sqrt{q^{2}}} \left[(M_{\Sigma^{0}} + M_{\Lambda}) F_{1}^{V} + \frac{q^{2}}{M_{\Sigma^{0}}} F_{2}^{V} \right] = \frac{\sqrt{Q_{-}}}{\sqrt{q^{2}}} (M_{\Sigma^{0}} + M_{\Lambda}) G_{E}$$

- F_1 and F_2 are the transition form factors, and $G_{\rm E/M}$ are electromagnetic form factors. $Q_+ = (M_{\Sigma^0} M_{\Lambda})^2 \pm q^2$
- G_E can be safely neglected because the electric radius is estimated to be much smaller than the magnetic one [2] [4], so as we do in MC generation.

[2]: Eur. Phys. J. C (2020) 80:218, 2020

[4]: Eur. Phys. J. A53:117, 2017



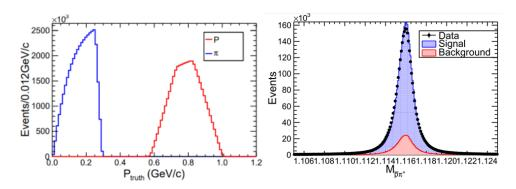
Event Selection

■ Good Tracks

- \triangleright $|\cos\theta| < 0.93$
- $> |V_z| < 30cm$
- $ightharpoonup N_{good} \ge 2$

\square PID (dE/dx + TOF)

- $ightharpoonup p: Prob(p) > Prob(\pi/K/e) \&\& P_{\bar{p}} > 0.55 \text{ GeV/}c$
- $ightharpoonup \pi$: $Prob(\pi) > Prob(p/K/e) \&\& P_{\pi} < 0.35 \text{ GeV}/c$
- $> N_{\bar{p}} \ge 1 \&\& N_{\pi^+} \ge 1$



□ Photon Selection

- Properties Opening angle between shower and the nearest charged track $> 10^{\circ}$ ($> 20^{\circ}$ for \bar{p})
- Barrel(Endcap): E > 25(50)MeV, $|\cos \theta| < 0.8(0.92)$
- > 0 < T < 14
- $> N_{\nu} \geq 1$

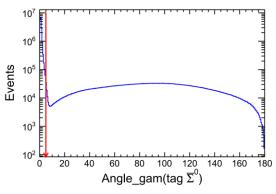
\Box $\overline{\Lambda}$ Reconstruction

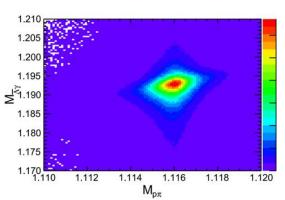
- Do vertex fit and secondary vertex fit of all $\bar{p}\pi^+$ combinations and choose the one with the minimum χ^2_{sec}
- $\blacktriangleright |M_{\bar{p}\pi^+} M_{\Lambda}| < 8 \text{MeV}/c^2$
- $\succ L_{decay} > 0$
- $> \chi_{sec}^2 < 200$

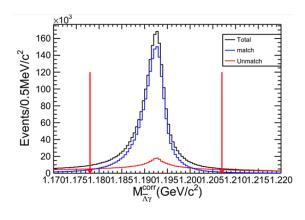


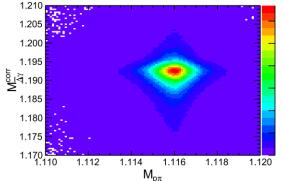
$\Box \overline{\Sigma}^0$ Reconstruction

- Looping all γ candidates, and keep the ones with the minimum value of $|M_{\overline{\Lambda}\gamma}^{corr}(M_{\overline{\Lambda}\gamma} M_{\overline{\rho}\pi^+} + M_{\Lambda})|$
- \triangleright Match angle between selected photon and truth information: $\theta_{match} < 5^{\circ}$
- $\left| M_{\overline{\Lambda} \gamma}^{corr} M_{\Sigma^0} \right| < 0.15 \text{GeV}/c^2$











Event Selection

□ Good Tracks

- \triangleright $|\cos\theta| < 0.93$
- $> |V_z| < 30cm$
- $> N_{good} \ge 6$

\square PID (dE/dx + TOF)

$$Prob(e) = \frac{Prob(e)}{Prob(e) + Prob(\pi) + Prob(K)} > 0.8$$

- $N_p \ge 1 \&\& N_{\pi^-} \ge 1$
- $N_{e^+} \ge 188N_{e^-} \ge 1$
- For e^{\pm} : $|V_r| < 1cm |V_z| < 10cm$

□ A Reconstruction

Reconstruction of Λ is the same as that of $\overline{\Lambda}$ on ST side

□ Kinematic Fit

- Firstly a vertex fit of e^+e^- is performed to improve e^+e^- kinematic uncertainties
- Loop all e^+e^- with γ , Λ , $\overline{\Lambda}$ to do 4C kinematic Fit, find the successfully fit ones with the minimum value of χ^2_{kmf} .



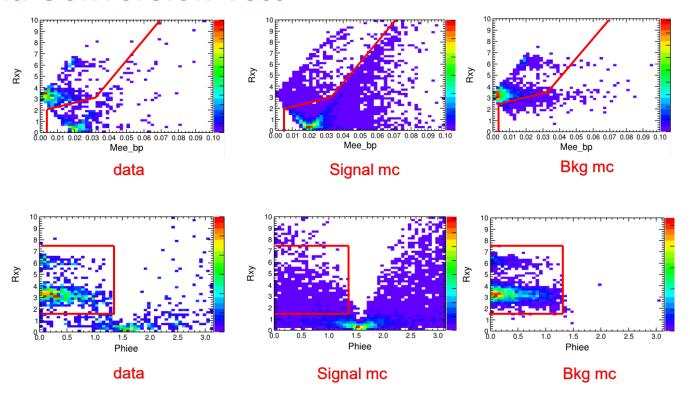
Table 1: Decay trees and their respective initial-final states.

rowNo	decay tree (decay initial-final states)	iDcyTr	iDcyIFSts	nEtr	nCEt
1	$J/\psi \to \Sigma^0 \bar{\Sigma}^0, \Sigma^0 \to \Lambda \gamma, \bar{\Sigma}^0 \to \bar{\Lambda} \gamma, \Lambda \to \pi^- p, \bar{\Lambda} \to \pi^+ \tilde{p}$ $(J/\psi \dashrightarrow \pi^+ \pi^- p \tilde{p} \gamma \gamma)$	0	0	427	427
2	$J/\psi \to \Sigma^0 \bar{\Sigma}^{*0}, \Sigma^0 \to \Lambda \gamma, \bar{\Sigma}^{*0} \to \pi^0 \bar{\Lambda}, \Lambda \to \pi^- p, \bar{\Lambda} \to \pi^+ \bar{p}$ $(J/\psi \dashrightarrow \pi^0 \pi^+ \pi^- p \bar{p} \gamma)$	1	1	3	430
3	$J/\psi \rightarrow \eta_c \gamma, \eta_c \rightarrow \Sigma^0 \bar{\Sigma}^0, \Sigma^0 \rightarrow \Lambda \gamma, \bar{\Sigma}^0 \rightarrow \bar{\Lambda} \gamma, \Lambda \rightarrow \pi^- p, \bar{\Lambda} \rightarrow \pi^+ \bar{p}$ $(J/\psi * \pi^+ \pi^- p \bar{p} \gamma \gamma \gamma)$	2	2	2	432
4	$J/\psi \to \Lambda \bar{\Sigma}^{*0}, \Lambda \to \pi^- p, \bar{\Sigma}^{*0} \to \pi^0 \bar{\Lambda}, \pi^0 \to e^+ e^- \gamma^F, \bar{\Lambda} \to \pi^+ \bar{p}$ $(J/\psi \dashrightarrow e^+ e^- \pi^+ \pi^- p \bar{p} \gamma^F)$	3	3	1	433
5	$J/\psi \to \Sigma^0 \bar{\Sigma}^0 \gamma, \Sigma^0 \to \Lambda \gamma, \bar{\Sigma}^0 \to \bar{\Lambda} \gamma, \Lambda \to \pi^- p, \bar{\Lambda} \to \pi^+ \bar{p}$ $(J/\psi * \pi^+ \pi^- p \bar{p} \gamma \gamma \gamma)$	4	2	1	434
6	$J/\psi \to \bar{\Lambda}\Sigma^{0}, \bar{\Lambda} \to \pi^{+}\bar{p}, \Sigma^{0} \to \Lambda\gamma, \Lambda \to \pi^{-}p$ $(J/\psi \dashrightarrow \pi^{+}\pi^{-}p\bar{p}\gamma)$	5	4	1	435
7	$J/\psi \to \Lambda \bar{\Sigma}^{*0}, \Lambda \to \pi^- p, \bar{\Sigma}^{*0} \to \pi^0 \bar{\Lambda}, \bar{\Lambda} \to \pi^+ \bar{p}$ $(J/\psi * \pi^0 \pi^+ \pi^- p \bar{p})$	6	5	1	436
8	$J/\psi \to \Lambda \bar{\Sigma}^0 \gamma, \Lambda \to \pi^- p, \bar{\Sigma}^0 \to \bar{\Lambda} \gamma, \bar{\Lambda} \to \pi^+ \bar{p}$ $(J/\psi - \to \pi^+ \pi^- p \bar{p} \gamma \gamma)$	7	0	1	437
9	$J/\psi \to \Lambda \bar{\Sigma}^{*0}, \Lambda \to \pi^- p, \bar{\Sigma}^{*0} \to \pi^0 \bar{\Lambda}, \pi^0 \to e^+ e^- \gamma^F \gamma^f, \bar{\Lambda} \to \pi^+ \bar{p}$ $(J/\psi \dashrightarrow e^+ e^- \pi^+ \pi^- p \bar{p} \gamma^F \gamma^f)$	8	6	1	438

From the analysis of DT inclusive topology, we can find that the most dominant background is $\Sigma^0 \to \Lambda \gamma$ from gamma conversion.



Gamma Conversion Veto



- $ightharpoonup \Phi_{ee} < 75^{\circ}$ when $2cm < R_{xy} < 7.5cm$ is rejected.
- Events on high mass side of the curve are selected. The curve is defined between $(0.004 \text{GeV}/c^2,0\text{cm}),(0.004 \text{GeV}/c^2,2\text{cm}),(0.03 \text{GeV}/c^2,3\text{cm}),(0.07 \text{GeV}/c^2,10\text{cm})$



Table 1: Decay trees and their respective initial-final states.

rowNo	decay tree (decay initial-final states)	iDcyTr	iDcyIFSts	nEtr	nCEtr
1	$\begin{array}{l} J/\psi \to \Sigma^0 \bar{\Sigma}^0, \Sigma^0 \to \Lambda \gamma, \bar{\Sigma}^0 \to \bar{\Lambda} \gamma, \Lambda \to \pi^- p, \bar{\Lambda} \to \pi^+ \bar{p} \\ (J/\psi \dashrightarrow \pi^+ \pi^- p \bar{p} \gamma \gamma) \end{array}$	0	0	427	427
2	$J/\psi \rightarrow \Sigma^0 \bar{\Sigma}^{*0}, \Sigma^0 \rightarrow \Lambda_{\gamma}, \bar{\Sigma}^{*0} \rightarrow \pi^0 \bar{\Lambda}, \Lambda \rightarrow \pi^- p, \bar{\Lambda} \rightarrow \pi^+ \bar{p}$ $(J/\psi \rightarrow \pi^0 \pi^+ \pi^- p \bar{p} \gamma)$	1	1	3	430
3	$\begin{array}{l} J/\psi \rightarrow \eta_c \gamma, \eta_c \rightarrow \Sigma^0 \tilde{\Sigma}^0, \Sigma^0 \rightarrow \Lambda \gamma, \tilde{\Sigma}^0 \rightarrow \bar{\Lambda} \gamma, \Lambda \rightarrow \pi^- p, \bar{\Lambda} \rightarrow \pi^+ \bar{p} \\ (J/\psi \rightarrow \pi^+ \pi^- p \bar{p} \gamma \gamma \gamma) \end{array}$	2	2	2	432
4	$\begin{array}{l} J/\psi \to \Lambda \bar{\Sigma}^{*0}, \Lambda \to \pi^- p, \bar{\Sigma}^{*0} \to \pi^0 \bar{\Lambda}, \pi^0 \to e^+ e^- \gamma^F, \bar{\Lambda} \to \pi^+ \bar{p} \\ (J/\psi \dashrightarrow e^+ e^- \pi^+ \pi^- p \bar{p} \gamma^F) \end{array}$	3	3	1	433
5	$J/\psi \rightarrow \Sigma^0 \bar{\Sigma}^0 \gamma, \Sigma^0 \rightarrow \Lambda \gamma, \bar{\Sigma}^0 \rightarrow \bar{\Lambda} \gamma, \Lambda \rightarrow \pi^- p, \bar{\Lambda} \rightarrow \pi^+ \bar{p}$ $(J/\psi \pi^+ \pi^- p \bar{p} \gamma \gamma \gamma)$	4	2	1	434
6	$J/\psi \rightarrow \bar{\Lambda}\Sigma^{0}, \bar{\Lambda} \rightarrow \pi^{+}\bar{p}, \Sigma^{0} \rightarrow \Lambda\gamma, \Lambda \rightarrow \pi^{-}p$ $(J/\psi \pi^{+}\pi^{-}p\bar{p}\gamma)$	5	4	1	435
7	$J/\psi \to \Lambda \bar{\Sigma}^{*0}, \Lambda \to \pi^- p, \bar{\Sigma}^{*0} \to \pi^0 \bar{\Lambda}, \bar{\Lambda} \to \pi^+ \bar{p}$ $(J/\psi \dashrightarrow \pi^0 \pi^+ \pi^- p\bar{p})$	6	5	1	436
8	$J/\psi \to \Lambda \bar{\Sigma}^0 \gamma, \Lambda \to \pi^- p, \bar{\Sigma}^0 \to \bar{\Lambda} \gamma, \bar{\Lambda} \to \pi^+ \bar{p}$ $(J/\psi \dashrightarrow \pi^+ \pi^- p \bar{p} \gamma \gamma)$	7	0	1	437
9	$J/\psi \rightarrow \Lambda \bar{\Sigma}^{*0}, \Lambda \rightarrow \pi^{-}p, \bar{\Sigma}^{*0} \rightarrow \pi^{0}\bar{\Lambda}, \pi^{0} \rightarrow e^{+}e^{-}\gamma^{F}\gamma^{f}, \bar{\Lambda} \rightarrow \pi^{+}\bar{p}$ $(J/\psi \rightarrow e^{+}e^{-}\pi^{+}\pi^{-}p\bar{p}\gamma^{F}\gamma^{f})$	8	6	1	438

Г	rowNo	decay tree (decay initial-final states)		iDeyIFSto		nCEtr
ĺ	1	$J/\psi \to \Sigma^0 \bar{\Sigma}^0, \Sigma^0 \to \Lambda \gamma, \bar{\Sigma}^0 \to \bar{\Lambda} \gamma, \Lambda \to \pi^- p, \bar{\Lambda} \to \pi^+ \bar{p} $ $(J/\psi \dashrightarrow \pi^+ \pi^- p \bar{p} \gamma \gamma)$	0	0	5	5
	2	$J/\psi \to \Lambda \Sigma^{+0}, \Lambda \to \pi^{-}p, \bar{\Sigma}^{+0} \to \pi^{0}\bar{\Lambda}, \pi^{0} \to e^{+}e^{-}\gamma^{F}, \bar{\Lambda} \to \pi^{+}\bar{p}$ $(J/\psi \dashrightarrow e^{+}e^{-}\pi^{+}\pi^{-}p\bar{p}\gamma^{F})$	1	1	1	6

Very Low Background Level after Conversion Cut!

Systematic Uncertainty



Source	$\Sigma^0 o \Lambda e^+ e^- (\%)$	$\bar{\Sigma}^0 \to \bar{\Lambda} e^+ e^- (\%)$	Combined(%)
$\Lambda(\bar{\Lambda})$ reconstruction	1.0	1.0	1.0
e^+ tracking	0.3	0.3	0.3
e^- tracking	0.4	0.4	0.4
e^+ PID	0.3	0.3	0.3
e^- PID	0.3	0.3	0.3
Gamma conversion veto	1.1	1.1	1.1
e^+e^- vertex fit and 4C kinematic fit	1.3	1.3	1.3
Single tag fit	1.5	0.6	1.1
Double tag fit	2.8	2.4	2.6
Total Uncertainty of $\Sigma^0(\bar{\Sigma}^0) \to \Lambda(\bar{\Lambda})e^+e^-$	3.8	3.3	3.5